Applied Physics Letters ARTICLE scitation.org/journal/apl

Deep learning model as an inversion tool for resonant ultrasound spectroscopy of piezoelectric materials

Cite as: Appl. Phys. Lett. **120**, 184101 (2022); doi: 10.1063/5.0086238
Submitted: 24 January 2022 · Accepted: 22 April 2022 ·
Published Online: 4 May 2022

Wuyi Yang,[1] Shanshan Sun,[1] Jing Hu,[1] Liguo Tang,[1,2,a)] Lei Qin,[3,a)] Zhenglin Li,[4] and Wenyu Luo[2,5]

AFFILIATIONS

[1]Key Laboratory of Underwater Acoustic Communication and Marine Information Technology, Ministry of Education, College of Ocean and Earth Sciences, Xiamen University, Xiamen 361010, China
[2]State Key Laboratory of Acoustics, Institute of Acoustics, Chinese Academy of Sciences, Beijing 100190, China
[3]Beijing Key Laboratory for Sensors, Beijing Information Science & Technology University, Beijing 100192, China
[4]School of Ocean Engineering and Technology, Sun Yat-sen University, Zhuhai 519000, China
[5]University of Chinese Academy of Sciences, Beijing 100049, China

[a)]**Authors to whom correspondence should be addressed:** liguotang@xmu.edu.cn and qinlei@bistu.edu.cn

ABSTRACT

Device fabrication based on piezoelectric materials requires prior characterization of full matrix constants. For this, the Institute of Electrical and Electronics Engineers standard on piezoelectricity suggests the use of ultrasonic pulse-echo and electric resonance methods. However, these techniques tend to provide inconsistent characterization, because they require multiple samples with drastically different sizes. Resonant ultrasound spectroscopy (RUS) is a promising alternative, because it uses only a single sample for characterization, thus ensuring self-consistent results. The inverse problem of finding material constants from resonant frequencies is often solved using the nonlinear least squares method despite its being a time-consuming algorithm. Herein, deep learning (DL) is introduced in the inversion procedure of RUS. After the DL network is trained, the material constants are determined with high efficiency. The practicability and reliability of the combination of DL and RUS are demonstrated by characterizing the full tensor constants of $LiNbO_3$ single crystals.

Piezoelectric materials, such as lead zirconate titanate (PZT), have been widely used as sensors and actuators since the 1950s.[1] Some new piezoelectric materials, such as relaxor-based ferroelectric single crystals, have also attracted extensive attention owing to their ultrahigh piezoelectric properties.[2,3] The design of sensors and actuators based on piezoelectric materials requires prior characterization of their elastic, piezoelectric, and dielectric constants. According to the Institute of Electrical and Electronics Engineers piezoelectric standard,[4] ultrasonic pulse-echo (UPE) and electric resonance (ER) methods are the two most widely used methods for determining the full matrix constants of piezoelectric materials. However, multiple rectangular parallelepiped samples with significantly different sizes must be used in these methods, which lead to inconsistent results. Moreover, preparing large and high-quality piezoelectric crystals for some piezoelectric materials is extremely difficult. For example, the maximum thickness of commercial $Bi_4Ti_3O_{12}$ (BIT) crystals produced by Fuji Ceramics Corporation is only 2 mm. The small size of the BIT sample limits the use of UPE and ER in its characterization.

To overcome the drawbacks of the UPE and ER methods, techniques that use only one sample to characterize the full matrix constants of piezoelectric materials must be developed. Moreover, these methods should be able to characterize small piezoelectric samples. Resonant ultrasound spectroscopy (RUS) is one such method.[5] In RUS, the resonance frequencies of a piezoelectric sample depend on its geometric and material constants, which can be determined if its resonance frequencies can be precisely measured and its geometric size is known.

RUS was first introduced by Frazer and LeCraw to characterize the elastic properties of a homogeneous sphere.[5] Ohno was the first to apply RUS to characterize the material constants of piezoelectric materials.[6] Ogi *et al.*[7–9] applied RUS to characterize the full tensor constants of some piezoelectric materials with very high mechanical quality factors (Q_M) such as lithium niobate, a-quartz, and GaN. Tang *et al.*[10]

characterized the temperature dependence of the full matrix material constants of $[001]_c$ poled Mn-doped 0.24PIN-0.46PMN-0.30PT single crystals using RUS. Zhuang *et al.*[11] also extended RUS to the nondestructive evaluation of the homogeneity of piezoelectric materials.

Inversion is one of the core procedures in RUS wherein the fundamental material constants are obtained from the measured resonance frequencies. The Levenberg–Marquardt (LM) algorithm, which is a nonlinear least squares (NLS) optimization method, is often used as the inversion algorithm in RUS. During the inversion, the calculation of resonance frequencies of the piezoelectric sample must be repeated dozens of times. These resonance frequencies can also be calculated using the finite element method or the Rayleigh–Ritz method.[12] However, these methods involve time-consuming calculations and a tedious code development process.

Deep learning (DL) has made remarkable breakthroughs in a wide range of practical machine learning tasks such as computer vision and natural language processing.[13,14] An important problem in DL is the implementation of a mapping to approximate a function. Based on a given set of input–output value pairs, a neural network can be learned to implement this through the backpropagation (BP) algorithm.[15] Hornik[16] showed that a single hidden layer neural network can effectively approximate continuous functions on bounded domains arbitrary. Deep networks are better than shallow networks at approximating functions, which can be expressed as a composition of functions.[17] In this Letter, we use DL to model the relationship between the resonance frequencies and material constants of the piezoelectric samples. We also aim to compare the material constant characterization and computational time of the deep learning model and the LM algorithm as inversion processes for RUS.

Hitherto, limited types of piezoelectric materials have been widely used such as PZT, relaxor-based ferroelectric single crystals, and lead-free piezoelectric materials. While most of these crystals are commonly characterized, the constants of the same type of material may slightly vary across manufacturers and production batches owing to different manufacturing technologies and conditions. This is a common phenomenon in relaxor-based ferroelectric single crystals. Consequently, a large number of calculated training samples can be generated based on known material constants. Therefore, RUS is a very good application area for DL. Once successfully trained, DL is also far more efficient than NLS as an inversion tool of RUS.

In this Letter, we demonstrate the practicability and reliability of DL in RUS by characterizing the full tensor constants of $LiNbO_3$ single crystals. The crystallographic symmetry of the X/Y/Z cut $LiNbO_3$ crystal is $3m$ below its Curie point. The matrices of the elastic, piezoelectric, and dielectric constants corresponding to crystals with a $3m$ symmetry are

$$[c^E] = \begin{bmatrix} c_{11}^E & c_{12}^E & c_{13}^E & c_{14}^E & 0 & 0 \\ c_{12}^E & c_{11}^E & c_{13}^E & -c_{14}^E & 0 & 0 \\ c_{13}^E & c_{13}^E & c_{33}^E & 0 & 0 & 0 \\ c_{14}^E & -c_{14}^E & 0 & c_{44}^E & 0 & 0 \\ 0 & 0 & 0 & 0 & c_{44}^E & c_{14}^E \\ 0 & 0 & 0 & 0 & c_{14}^E & \frac{1}{2}\left(c_{11}^E - c_{12}^E\right) \end{bmatrix}, \quad (1)$$

$$[e] = \begin{bmatrix} 0 & 0 & 0 & 0 & e_{15} & -e_{22} \\ -e_{22} & e_{22} & 0 & e_{15} & 0 & 0 \\ e_{31} & e_{31} & e_{33} & 0 & 0 & 0 \end{bmatrix}, \quad (2)$$

and

$$[\varepsilon^S] = \begin{bmatrix} \varepsilon_{11}^S & 0 & 0 \\ 0 & \varepsilon_{11}^S & 0 \\ 0 & 0 & \varepsilon_{33}^S \end{bmatrix}, \quad (3)$$

respectively.

The RUS experimental setup is the same as that presented in Ref. 13. The dimensions and density of the $LiNbO_3$ sample were $5.055 \times 5.041 \times 5.033\ mm^3$ and $4633\ kg/m^3$, respectively. During the measurement of the resonant ultrasound spectra, the sample was placed between the transmitting and receiving transducers with contact only at the opposite corners. Because the sample position had a significant influence on the measurement, some resonance modes appeared in one measurement but disappeared in another. Multiple measurements were necessary to reduce mode omission. As an example, the red and blue lines in Fig. 1 are the results of two different measurements. Each peak in Fig. 1 corresponds to the resonance frequency. The third and sixth resonance modes can be easily identified from the red line, but they cannot be identified from the blue line.

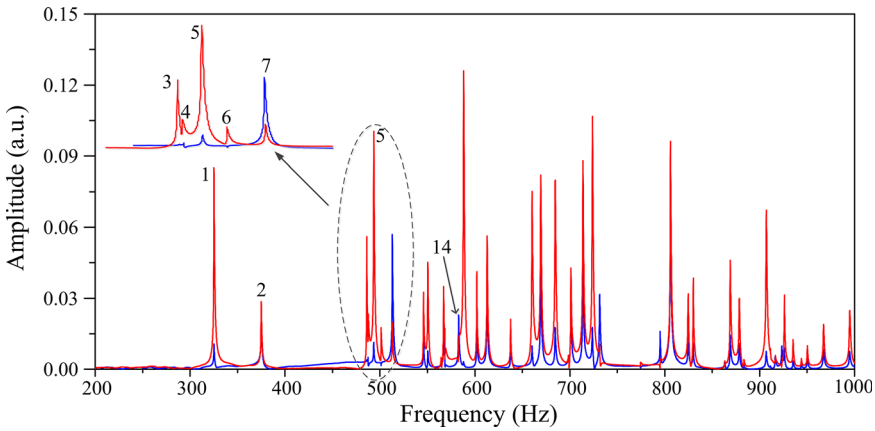

FIG. 1. Measured resonant ultrasound spectra from 200 to 1000 kHz corresponding to the rectangular parallelepiped $LiNbO_3$ sample. The red and blue lines are from two different measurements of the same sample.

However, the 14th resonance mode can be identified from the blue line, but it cannot be identified from the red line. Table I lists the resonance frequencies f_{meas} identified from the measured resonant ultrasound spectra.

The clamped dielectric constants ε_{11}^S and ε_{33}^S were obtained from the high-frequency capacitance at 30 MHz measured using an HP4194A impedance analyzer with an HP16043E fixer. The relative dielectric constants $\varepsilon_{11}^S/\varepsilon_0$ and $\varepsilon_{33}^S/\varepsilon_0$ of the sample were 45 and 26,

TABLE I. Measured and calculated resonance frequencies, where f_{meas} corresponds to measured frequencies and f_{LM} and f_{DL} correspond to frequencies calculated using the constants determined by RUS using LM and DL, as shown in Table II.

	f_{meas}	f_{LM}	$diff_1$[a]	f_{DL}	$diff_2$[b]		f_{meas}	f_{LM}	$diff_1$[a]	f_{DL}	$diff_2$[b]
1	324.876	324.519	0.11	324.876	0.12	41	927.128	926.758	0.04	927.129	0.00
2	374.800	374.322	0.13	374.801	0.05	42	934.929	935.934	0.11	934.929	0.05
3	485.905	486.075	0.04	485.906	0.01	43	945.336	944.220	0.12	945.336	0.05
4	487.798	488.092	0.06	487.799	0.02	44	950.070	948.335	0.18	950.071	0.08
5	493.045	493.081	0.01	493.045	0.14	45	965.808	964.973	0.09	965.809	0.03
6	501.309	502.118	0.16	501.309	0.33	46	993.964	992.809	0.12	993.965	0.05
7	513.243	513.548	0.06	513.243	0.15	47	1011.58	1010.63	0.09	1011.58	0.12
8	545.489	546.768	0.23	545.489	0.39	48	1036.76	1036.94	0.02	1036.76	0.07
9	550.329	550.131	0.04	550.329	0.24	49	1044.51	1045.75	0.12	1044.51	0.18
10	564.444	565.051	0.11	564.444	0.03	50	1045.36	1046.44	0.10	1045.36	0.11
11	566.797	567.683	0.16	566.797	0.18	51	1050.27	1052.15	0.18	1050.27	0.19
12	568.238	568.413	0.03	568.238	0.04	52	1061.69	1062.00	0.03	1061.70	0.06
13	568.913	568.861	0.01	568.913	0.02	53	1064.15	1064.28	0.01	1064.15	0.08
14	582.445	582.854	0.07	582.445	0.04	54	1074.13	1075.52	0.13	1074.13	0.22
15	587.793	587.287	0.09	587.794	0.09	55	1076.31	1076.88	0.05	1076.31	0.10
16	601.832	602.905	0.18	601.832	0.39	56	1090.11	1090.53	0.04	1090.11	0.07
17	613.004	612.401	0.10	613.004	0.08	57	1098.52	1097.67	0.08	1098.52	0.07
18	638.324	638.470	0.02	638.324	0.02	58	1099.09	1099.83	0.07	1099.00	0.18
19	660.159	659.974	0.03	660.160	0.22	59	1106.97	1106.71	0.02	1106.97	0.04
20	669.544	669.554	0.00	669.544	0.06	60	1116.36	1116.40	0.00	1116.36	0.03
21	683.336	683.220	0.02	683.337	0.05	61	1120.33	1120.96	0.06	1120.60	0.03
22	698.218	697.922	0.04	698.218	0.08	62	1124.56	1124.53	0.00	1123.50	0.04
23	700.596	700.151	0.06	700.596	0.03	63	1126.35	1126.73	0.03	1126.35	0.02
24	714.062	713.115	0.13	714.062	0.15	64	1128.71	1128.52	0.02	1128.30	0.10
25	723.253	722.290	0.13	723.253	0.00	65	1138.27	1138.59	0.03	1138.27	0.00
26	730.803	731.770	0.13	730.803	0.24	66	1141.65	1141.60	0.00	1141.65	0.03
27	774.544	775.060	0.07	774.545	0.13	67	1146.92	1146.54	0.03	1146.92	0.00
28	795.046	796.131	0.14	795.046	0.16	68	1149.11	1148.87	0.02	1148.20	0.17
29	805.893	806.684	0.10	805.894	0.07	69	1154.10	1154.46	0.03	1154.10	0.04
30	813.045	812.809	0.03	813.045	0.06	70	1154.53	1155.30	0.07	1154.53	0.06
31	824.334	824.668	0.04	824.334	0.03	71	1159.17	1158.21	0.08	1159.17	0.08
32	830.003	830.370	0.04	830.003	0.02	72	1163.39	1163.20	0.02	1163.39	0.06
33	863.079	861.779	0.15	863.079	0.06	73	1165.69	1163.98	0.15	1165.69	0.13
34	869.594	869.603	0.00	869.595	0.04	74	1171.97	1171.27	0.06	1171.97	0.04
35	877.808	878.594	0.09	877.808	0.07	75	1188.04	1188.80	0.06	1188.04	0.12
36	883.723	883.249	0.05	883.724	0.02	76	1204.26	1202.13	0.18	1204.26	0.13
37	905.304	906.274	0.11	905.305	0.15	77	1216.26	1216.53	0.02	1216.26	0.08
38	911.298	912.688	0.15	911.299	0.18	78	1217.34	1217.96	0.05	1217.34	0.11
39	916.553	917.065	0.06	916.553	0.09	79	1227.94	1225.76	0.18	1227.94	0.06
40	922.652	922.654	0.00	922.652	0.06	80	1239.83	1241.40	0.13	1239.83	0.20

[a]Diff $= \left|\frac{f_{meas}-f_{LM}}{(f_{meas}+f_{LM})/2}\right| \times 100.$

[b]Diff $= \left|\frac{f_{meas}-f_{DL}}{(f_{meas}+f_{DL})/2}\right| \times 100.$

TABLE II. Material constants c_{ij}^{E} and e_{ij} determined by RUS using LM and DL.

	Elastic stiffness constants (10^{10} N/m^2)						Piezoelectric stress constants (C/m^2)			
	c_{11}^{E}	c_{12}^{E}	c_{13}^{E}	c_{14}^{E}	c_{33}^{E}	c_{44}^{E}	e_{15}	e_{22}	e_{31}	e_{33}
LM	19.94	5.53	6.88	0.774	23.63	6.03	3.56	2.36	0.218	1.70
DL	20.03	5.47	6.86	0.776	23.67	6.04	3.55	2.36	0.208	1.67
Relative deviation (%)	0.45	1.09	0.29	0.26	0.17	0.17	0.28	0.00	4.69	1.78

respectively. NLS is generally used to perform the inversion in RUS, the core of which is to find a local minimizer of the error function

$$F = \frac{1}{2}\sum_{i=1}^{K} w_i \left[f_{cal}^{(i)} - f_{meas}^{(i)}\right]^2, \tag{4}$$

where w_i is the weighting factor for different modes and $f_{meas}^{(i)}$ and $f_{cal}^{(i)}$ are the ith measured and calculated resonance frequencies, respectively.

Table II presents the inversion results of the elastic constants c_{ij}^{E} and piezoelectric constants e_{ij} using LM and DL. The first 127 resonance modes were used in the inversion. The elastic and piezoelectric constants given in Ref. 7 were used by LM as the initial values. f_{LM} in Table I denotes the resonance frequencies calculated using the constants determined by RUS using LM, as presented in Table II. The relative deviations between f_{meas} and f_{LM} are listed in Table I. Except for the eighth mode, all values are less than 0.2%, which indicate the preciseness of the inversion results.

We also investigated the sensitivity of the resonant frequencies to different material constants to determine which constants can be accurately determined using RUS. To investigate the influence of each material constant on different modes, the resonant frequencies were computed by changing the value of a particular constant with the other constants fixed. The dimensions, density, and dielectric constants of the sample used in the computation were the same as those stated above. The elastic and piezoelectric constants listed in Table II were used in the computations. Figure 2 shows the influence of the elastic constants on the resonance frequencies. Figure 3 shows the influence of the piezoelectric and dielectric constants on the resonance frequencies.

Figures 2(a)–2(c), 2(e), and 2(f) show that there were several modes that were sensitive to the elastic stiffness constants c_{11}^{E}, c_{12}^{E}, c_{13}^{E}, c_{33}^{E}, and c_{44}^{E}. For example, modes 6, 16, 20, 21, and 24 were extremely sensitive to c_{11}^{E}. As seen in Figs. 3(a) and 3(b), several modes were also highly sensitive to the piezoelectric constants e_{15} and e_{22}. For example, modes 7, 8, 15, and 23 were very sensitive to e_{15}. Compared with c_{11}^{E},

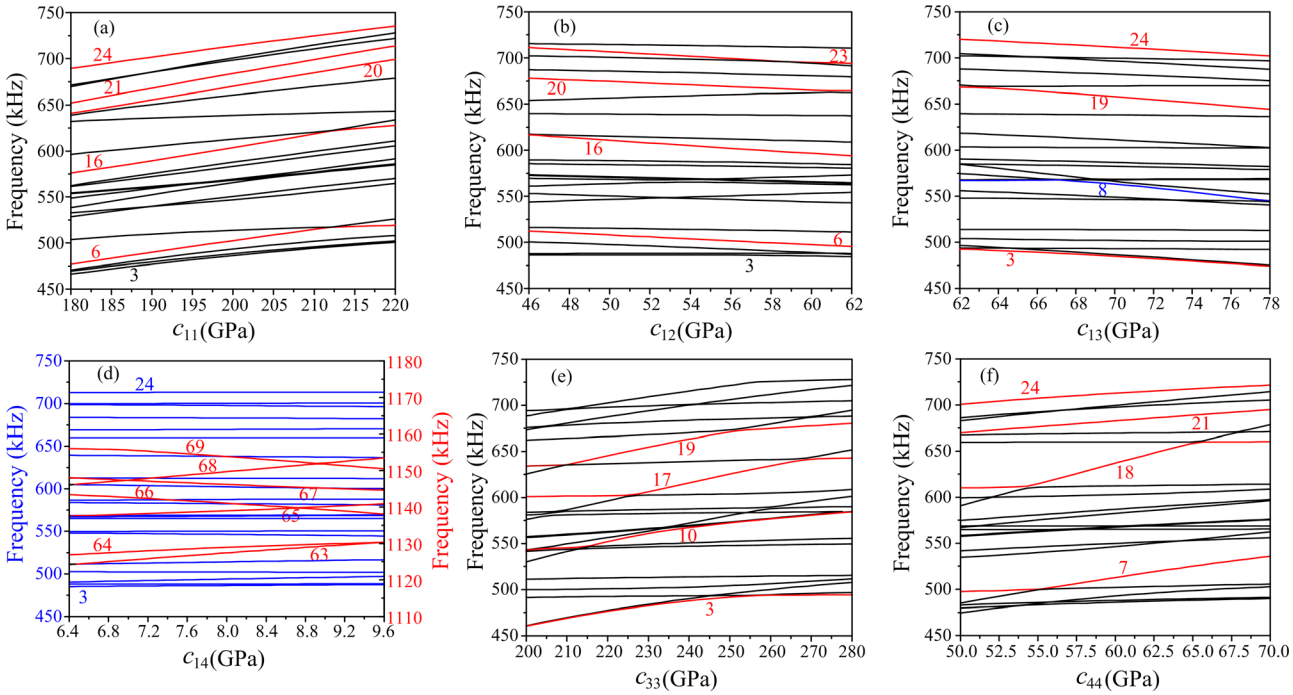

FIG. 2. Resonance frequencies as functions of elastic constants. (a) c_{11}^{E}, (b) c_{12}^{E}, (c) c_{13}^{E}, (d) c_{14}^{E}, (e) c_{33}^{E}, and (f) c_{44}^{E}.

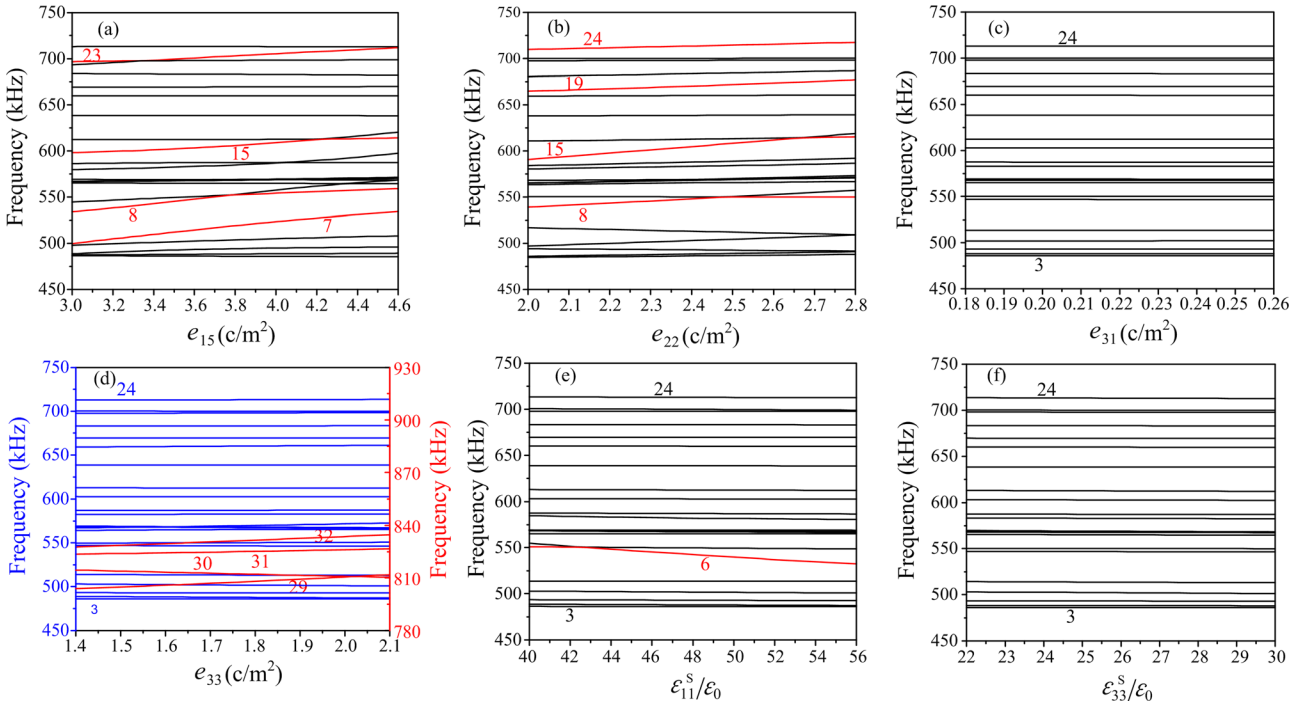

FIG. 3. Resonance frequencies as functions of piezoelectric and dielectric constants. (a) e_{15}, (c) e_{22}, (c) e_{31}, (d) e_{33}, (e) ε_{11}^S, and (f) ε_{33}^S.

c_{12}^E, c_{13}^E, c_{33}^E, c_{44}^E, e_{15}, and e_{22}, most modes were less sensitive to c_{14}^E and e_{33}. Compared with the constants that have a significant influence on resonance frequencies, more resonance modes are needed to determine a constant that has a weak influence on the resonance frequencies. Therefore, more resonance frequencies are needed to precisely determine c_{14}^E and e_{33} compared with c_{11}^E, c_{12}^E, c_{13}^E, c_{33}^E, c_{44}^E, e_{15}, and e_{22}. Figures 3(c), 3(e), and 3(f) show that most modes were insensitive to the piezoelectric constant e_{31} and dielectric constants ε_{11}^S and ε_{33}^S. Thus, they were difficult to determine using RUS. Fortunately, the values of ε_{11}^S and ε_{33}^S can be obtained from the capacitance measurements.

A total of M piezoelectric samples with different elastic stiffness constants and piezoelectric stress constants were randomly generated. Assuming the value of one elastic stiffness constant is ϑ, we set any elastic stiffness constant of a piezoelectric sample to a value randomly generated from a continuous uniform distribution in the interval $[\alpha\vartheta, \beta\vartheta]$. In this study, α and β were set as 0.9 and 1.1, respectively. The same process was used to randomly generate the piezoelectric stress constants of the piezoelectric sample. The resonance frequencies of these M piezoelectric samples were calculated using the Rayleigh–Ritz method.

Figure 4 shows the deep network structure used to model the relationship between the normalized resonance frequencies and the normalized material constants of the piezoelectric samples. The deep network structure comprises three fully connected neural sub-networks G_1

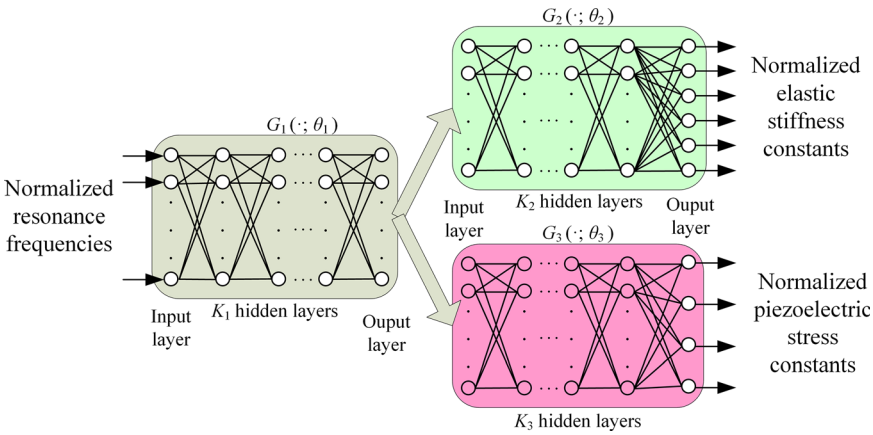

FIG. 4. Deep network structure comprising three deep neural sub-networks. The output of $G_1(\cdot;\theta_1)$ is the input of $G_2(\cdot;\theta_3)$ and $G_3(\cdot;\theta_3)$.

TABLE III. Proportion of samples with relative error of material constants in different intervals.

Relative error	Proportion of samples									
	c_{11}^E	c_{12}^E	c_{13}^E	c_{14}^E	c_{33}^E	c_{44}^E	e_{15}	e_{22}	e_{31}	e_{33}
<0.5%	89.04	61.03	68.68	43.54	72.44	81.55	65.60	52.47	5.67	36.68
0.5%–1%	9.51	25.13	25.37	28.70	22.66	14.29	25.55	31.80	5.94	27.72
1%–2%	1.45	9.96	5.79	19.64	4.74	2.94	7.95	14.76	11.16	25.95
2%–3%	0.01	2.69	0.16	5.28	0.15	0.74	0.88	0.94	11.48	7.15
3%–4%	0.00	0.94	0.00	1.84	0.02	0.35	0.03	0.01	11.00	1.71
4%–5%	0.00	0.22	0.00	0.57	0.00	0.11	0.00	0.00	10.69	0.56
>5%	0.00	0.04	0.00	0.42	0.00	0.01	0.00	0.00	44.06	0.22

$(\cdot;\theta_1)$, $G_2(\cdot;\theta_2)$, and $G_3(\cdot;\theta_3)$, where θ_1, θ_2, and θ_3 are the parameters of the sub-networks. The output of $G_1(\cdot;\theta_1)$ is the input of $G_2(\cdot;\theta_2)$ and $G_3(\cdot;\theta_3)$. In the nth sub-network, the number of hidden layers is K_n, the input layer is layer 0, the output layer is layer K_n+1, and N_i^n is the number of neurons at layer i, $i=0,\ldots,K_n+1$. We have $N_0^1=P$, $N_{K_1+1}^1=N_0^2=N_0^3$, $N_{K_2+1}^2=6$, and $N_{K_3+1}^3=4$. Leaky rectified linear units (ReLUs) were selected as the activation functions. Moreover, the activation function was not applied to the output layers of $G_2(\cdot;\theta_2)$ and $G_3(\cdot;\theta_3)$. The input of $G_1(\cdot;\theta_1)$ is the normalized resonance frequency vector. The outputs of $G_2(\cdot;\theta_2)$ and $G_3(\cdot;\theta_3)$ are the normalized elastic and piezoelectric constants, respectively.

The number of resonance frequencies was 127. The three sub-networks G_1, G_2, and G_3 shown in Fig. 4 have three, five, and five hidden layers, respectively. The number of network neurons is set as follows: $N_1^1=N_2^1=N_3^1=N_4^1=256$, $N_1^2=N_2^2=256$, $N_3^2=N_4^2=N_5^2=128$, $N_1^3=N_2^3=256$, and $N_3^3=N_4^3=N_5^3=128$. A total of 82 600 piezoelectric samples were randomly generated to learn the model parameters. Batch normalization was applied to accelerate deep network training. The TensorFlow library was used to generate a deep neural network structure. A fivefold validation procedure was applied to assess the performance of the network. In this procedure, 80% of the piezoelectric samples constituted a training dataset that was used to tune the network parameters, and 20% constituted a testing dataset that was used to test its performance.

The performance of the network structure was evaluated based on the relative error between the true value ϑ and estimated value ϑ^* of the material constants

$$re(\vartheta^*,\vartheta)=100\times\frac{|\vartheta^*-\vartheta|}{\vartheta}\%. \tag{5}$$

The proportion of samples with the relative errors of the material constants at different intervals is presented in Table III. The relative error between the true value and the estimated value of the material constant e_{31} is significant, because most modes were insensitive to the piezoelectric constant e_{31}, as shown in Fig. 3(c).

Table II lists the elastic constants c_{ij}^E and piezoelectric constants e_{ij} determined using the trained network. f_{DL} in Table I corresponds to the resonance frequencies calculated using the constants determined by the trained network. The relative errors between f_{meas} and f_{DL} are listed in Table I. All are less than 0.3%, except for the 8th and 16th modes.

Here, 82 600 training samples were randomly generated, which means that the calculation of resonance frequencies using the Rayleigh–Ritz method should be repeated 82 600 times. Therefore, the generation of training samples used in DL was time consuming. Experiments were performed on a desktop computer with an Intel i7–8565U CPU and 16 GB of RAM. The average training time of the network was approximately 15 min. However, the material constants could be determined using the trained network with high efficiency with the inversion procedure requiring only 150 ms on average. On the other hand, the inversion based on LM required tens of minutes or even several hours. If there were l constants to be determined using RUS, the calculation of the sample resonance frequencies had to be repeated $2l$ times in each iterative step of LM to obtain the Jacobi matrix, which is time consuming.

Except for c_{12}^E, e_{31}, and e_{33}, the relative deviations between all material constants determined using LM and DL were less than 0.5%, as presented in Table II. The piezoelectric constant e_{31} of the $LiNbO_3$ single-crystal sample could not be precisely determined using LM or DL, because most resonance modes were very insensitive to it, as shown in Fig. 2. This led to a large relative deviation between the LM and DL results corresponding to e_{31}. The relative errors between f_{meas} and f_{LM} corresponding to most resonance modes were less than 0.2%, whereas those between f_{meas} and f_{DL} corresponding to most resonance modes were less than 0.3%, as presented in Table I. In summary, the precision of the results obtained using DL was comparable to that obtained using LM. The time consumed in computing training samples was far more than that consumed in an inversion procedure based on LM. However, for a piezoelectric material manufacturer, many piezoelectric samples from different batches must be characterized. Once the DL model has been trained successfully, it can be repeatedly used with very high efficiency. Therefore, for commercial application, the inversion method based DL is far more efficient than that based on LM.

This work was supported by the National Natural Science Foundation of China (Grant Nos. U2006218, 11874061, and 11674270); State Key Laboratory of Acoustics, Chinese Academy of Science (Grant No. SKLA202108); and Open Research Fund of the Key Laboratory of Sensors, Beijing Information Science and Technology University. The authors thank H. M. Zhu (Xiamen University) for her help in the preparation of the $LiNbO_3$ sample.

AUTHOR DECLARATIONS

Conflict of Interest

The authors have no conflicts to disclose.

Author Contributions

W.Y. and S.S. contributed equally to this work.

DATA AVAILABILITY

The data that support the findings of this study are available from the corresponding authors upon reasonable request.

REFERENCES

[1]B. Jaffe, W. R. Cook, and H. Jaffe, *Piezoelectric Ceramics* (Academic Press, 1971).
[2]S. J. Zhang and F. Li, J. Appl. Phys. **111**, 031301 (2012).
[3]E. W. Sun, R. Zhang, F. M. Wu, and W. W. Cao, J. Alloys Compd. **553**, 267 (2013).
[4]*IEEE Standard on Piezoelectricity, ANSI/IEEE Std 176* (IEEE, 1987).
[5]D. B. Frazer and R. C. LeCraw, Rev. Sci. Instrum. **35**, 1113 (1964).
[6]I. Ohno, Phys. Chem. Miner. **17**, 371 (1990).
[7]H. Ogi, Y. Kawasaki, M. Hirao, and H. Ledbetter, J. Appl. Phys. **92**, 2451 (2002).
[8]H. Ogi, T. Ohmori, N. Nakamura, and M. Hirao, J. Appl. Phys. **100**, 053511 (2006).
[9]N. Nakamura, H. Ogi, and M. Hirao, J. Appl. Phys. **111**, 013509 (2012).
[10]L. G. Tang, H. Tian, Y. Zhang, and W. W. Cao, Appl. Phys. Lett. **108**, 082901 (2016).
[11]M. H. Zhuang, L. G. Tang, R. Zhu, and G. S. Xu, J. Phys. D: Appl. Phys. **53**, 035303 (2020).
[12]R. Holland and E. P. Eer Nisse, IEEE Trans. Sonics Ultrason. **SU-15**, 119 (1968).
[13]A. Krizhevsky, I. Sutskever, and G. E. Hinton, Commun. ACM **60**, 84 (2017).
[14]A. Graves, A. R. Mohamed, and G. Hinton, in 2013 ICASSP, 2013.
[15]D. E. Rumelhart, G. E. Hinton, and R. J. Williams, Nature **323**, 533 (1986).
[16]K. Hornik, Neural Netw. **4**, 251 (1991).
[17]H. N. Mhaskar and T. Poggio, Anal. Appl. **14**, 829 (2016).